This article has been accepted for publication in a future issue of this journal, but has not been fully edited. Content may change prior to final publication. Citation information: DOI 10.1109/LRA.2020.2967318, IEEE Robotics and Automation Letters



# A Device for Rapid, Automated Trimming of Insect-Sized Flying Robots

Daksh Dhingra[1], Yogesh M. Chukewad[1] and Sawyer B. Fuller[1]

***Abstract*—Successful demonstrations of controlled flight in flying insect-sized robots (FIRs) <500 mg have all relied on piezo-actuated flapping wings because of unfavorable downward size scaling in motor-driven propellers. In practice, the mechanical complexity of flapping wings typically results in large torque bias variability about pitch and roll axes, leading to rapid rotation in free flight for vehicles that are not properly trimmed. Manual trimming by watching high-speed video is tedious and error-prone. In this letter, we introduce an alternative, a trimming device that uses feedback from motion capture cameras to determine and correct for bias torques. It does so using an automated feedback loop, without the need for any visual feedback from the user, or airborne flights which can damage the robot. We validated the device on two different robot flies. After trimming with our device, the robots both took off approximately vertically in open-loop and were able to hover in free flight under feedback control. Our system, therefore, reduces the time of essential yet time-consuming step in robot fly fabrication, facilitating their eventual mass production and practical application.**

***Index Terms*—Micro/Nano Robots, Automation at Micro-Nano Scales, Aerial Systems: Mechanics and Control**

## I. INTRODUCTION

DUE to their small size and ability to explore confined spaces, flying insect-sized robots (FIRs) can be used in search and rescue missions. And they are inexpensive and extremely lightweight—with a mass measured in milligrams—making them an appealing alternative to large rovers for space exploration. They might also be used for crop monitoring in farming applications.

The first feedback-controlled flying insect robot (FIR) was demonstrated in [1]. Since then, improvements to the basic design have explored increasing payload capacity, simplifying fabrication, and achieving passive attitude stability. In [2] the effect of relative position between the aerodynamics center and center of gravity on intrinsic attitude stability of the FIR was studied, and [3] provided a better understanding of the dynamics of a flapping wing mechanism. In [4] a four-wing design with increased payload capacity and steering actuation was demonstrated, while [5] introduced an alternative design actuated by uniomorph actuators. To expand the mobility of robot flies, [6] improved the design by reducing part count and lowering the center of mass, allowing landing and ground ambulation in addition to flight. This design was further modified using a set of three leg appendages in [7] to facilitate air-water surface locomotion. An emerging alternative to flapping wings also suited to insect scale is miniaturized electrohydrodynamic thrust introduced in [8] and [9].

Manuscript received: September, 10, 2019; Revised December, 7, 2019; Accepted December, 27, 2019.

This paper was recommended for publication by Editor Xinyu Liu upon evaluation of the Associate Editor and Reviewers' comments.

[1] Daksh Dhingra, Yogesh M. Chukewad, and Sawyer B. Fuller are with the Department of Mechanical Engineering, University of Washington, Seattle, USA dd292@uw.edu

Digital Object Identifier (DOI): see top of this page.

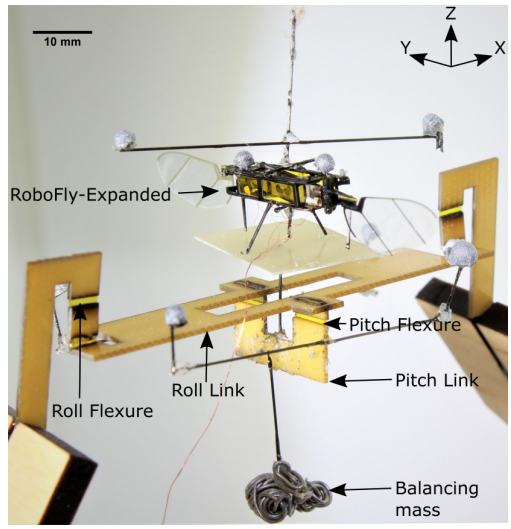


Fig. 1: A Robofly is shown mounted on the reported trimming device. The device restricts all degrees of freedom except pitch and roll rotation, which occur through laser-microfabricated flexure joints joined by rigid links. A balancing mass at bottom ensures that the system is at equilibrium in the upright orientation. Using this device, torque biases arising due to manufacturing irregularity can be detected and compensated for through an automated process.

Each of the foregoing FIR flight demonstrations required that the robot be trimmed, regardless of the number of actuators or design of the robot. From undergraduate physics, an arbitrary set of forces and torques acting on a rigid body can be decomposed into a single force vector acting at its center of mass, and a torque vector. For flight control, we can make two statements about the force and torque acting on a properly-trimmed hovering device such as the Robofly [6]:

1) A zero commanded torque should result in zero net rotational acceleration.
2) A thrust force should result in a zero net lateral acceleration in the body frame.

Here, we are primarily concerned with (1) above, because a non-zero bias torque results in relatively much larger flight path deviations, which make it hard to correct for in free-flight [1], [4], [10].

In the context of small flapping-wing robots like FIRs, trimming at such small scales entails two challenges that distinguish it from larger vehicles: (1) Rotational acceleration rates increase as size scale diminishes [11], [12], making the

2377-3766 (c) 2019 IEEE. Personal use is permitted, but republication/redistribution requires IEEE permission. See http://www.ieee.org/publications_standards/publications/rights/index.html for more information.

This article has been accepted for publication in a future issue of this journal, but has not been fully edited. Content may change prior to final publication. Citation information: DOI 10.1109/LRA.2020.2967318, IEEE Robotics and Automation Letters



dynamics of small vehicles particularly fast. The challenge is exacerbated by the fact that, like many flying insects including fruit flies and hawkmoths, their dynamics are unstable [3], [12], [13]. And (2) being based predominantly on flapping wings, FIRs consist of a flapping mechanism that, by virtue of its novelty, small size, and complexity, is subject to greater variability in performance than, for example, slightly larger quad-rotor helicopters. The result is that the magnitude of compensatory trim required is larger. As a result, in almost all cases, the first open-loop flights of such robots without trimming result in rapid inversion and a subsequent crash. If the vehicle does take off, it typically moves too far—out of the range of tracking cameras—before the controller is able to adapt for and correct for this irregularity. The trimming device we introduce in this work addresses both challenges.

For this work, we define the torque trimming process to be the task of finding a trim torque, $\tau_t$, that exactly cancels the non-zero bias torque $\tau_b$. A bias torque $\tau_b$ can arise from a) manufacturing inconsistencies, b) wear, and c) if there is damage to the FIR. The bias torque varies from robot to robot, as well as with changes in the payload carried by the robot, like a camera [14], boost converters for onboard power in [15], or an array of photovoltaic cells in [16], making trimming necessary for each robot. In current practice [4], [6], [10], [17], trimming was performed by filming short flights <0.5 s using a high speed camera. The magnitude and direction of the bias torque vector were estimated manually by observing the slow-motion videos. This method requires many human handled, unstable, and thus crash-prone flights.

In this letter, we introduce a new purpose-designed apparatus that can trim FIRs precisely, rapidly, and automatically. In addition to reducing the operator time it takes to trim a robot, our trimming device reduces the amount of wear and tear on the robot. In comparison, trimming using open-loop takeoffs from the ground invariably involves impacts to the wings, and requires manual handling to re-right the vehicle, which often entails an even greater chance of damage. It is also possible to trim a vehicle hanging from a thin kevlar filament, eliminating wing impacts, but this brings its own set of problems including damage when the wing becomes entangled in this filament, and it is often difficult to disambiguate, in video footage, torques due to torque baises versus those arising from tension on the filament.

In our device, trimming is performed using closed-loop feedback. While the wings are flapped, a controller receives Euler Angles in real-time and continuously updates trim values to counteract bias torques. The device allows us to minimize two quantities: the pitch bias torque $\tau_b^{pitch}$ and the roll bias torque $\tau_b^{roll}$. After doing so, the robot lifts off nearly vertically. This effectively places the flying system's state within the stability basin of our closed-loop free-flight controller. In the remainder of this report, we describe the design, operation, and testing of this new apparatus.

## II. Principles of Operation

The concept of trimming was first introduced in the ships [18] for achieving the desired velocity and direction. This

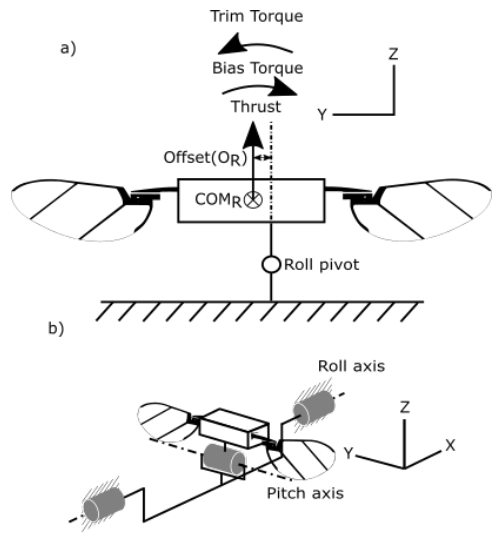


Fig. 2: (a) A 2D representation of forces and torques acting on the robot attached to a single-axis version of the trimming device. The robot is constrained to rotate freely around a single axis; assuming $O_R$ can be made small, the trim device rotates in response to a bias torque, which can be corrected by adding a compensatory trim torque. (b) A 3D representation of the rotation axes of the two-axis trimming device reported here, which allows trimming roll and pitch axes simultaneously.

term was later adopted by the aviation community to indicate the process of moving onboard freight and trim tabs to achieve a stable flight condition. Trim analysis is a very fundamental and essential procedure in flight mechanics. Formally defined in [19], trim is a flight condition in which the rate of change of the state vector of an aircraft is zero when there are no net applied forces and moments. This definition holds a different significance depending on the type of air vehicle. In helicopters, [20] trimming analysis is a vital part of a stable flight and mid-air maneuvering, this is achieved by using three independent control inputs for the main rotor and one for the tail rotor. In airplanes, trim tabs are provided to a pilot for adjusting stick and rudder paddle forces [19]. In quad-rotor helicopters, pitch and roll trim is typically performed by adjusting the relative speeds of the rotors to compensate for weight or thrust imbalance. In FIRs, trimming consists of altering the wing kinematics so that there is zero net torque applied.

### A. Trimming About an Elastic Rotation Axis

Torque sensing is commonly achieved by measuring small rotational deflections. One approach is to create a rigid system with sensors capable of detecting small deflections, e.g. the Nano17 Titanium (ATI Industrial Automation, NJ, USA). While this provides high bandwidth, the 8 $\mu$Nm resolution is insufficient. Capacitive pickup is an alternative that has demonstrated sufficient precision [21], but requires costly electronics hardware and has not been demonstrated in two axes. Our approach is to instead use a low-stiffness spring. This sacrifices unneeded bandwidth in exchange for large deflections that can be measured using sensors commonly

2377-3766 (c) 2019 IEEE. Personal use is permitted, but republication/redistribution requires IEEE permission. See http://www.ieee.org/publications_standards/publications/rights/index.html for more information.

This article has been accepted for publication in a future issue of this journal, but has not been fully edited. Content may change prior to final publication. Citation information: DOI 10.1109/LRA.2020.2967318, IEEE Robotics and Automation Letters



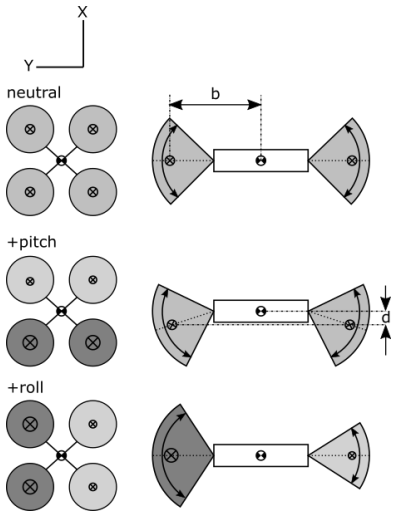


Fig. 3: A comparison of the mechanisms by which quad-rotor aircraft and the Robofly actuate pitch and roll torques. The centers of aerodynamic thrust are denoted by a $\otimes$ with a size proportional to thrust magnitude

available in a robotics laboratory such as a motion capture system or accelerometer and can be built using the same processes used to fabricate the robot itself.

We begin by introducing the underlying physics of a flying robot attached to a trimming device of our design, whose basic form is shown in Fig. 2(b). The principle of operation relies on the fact that the device constrains the robot to rotate around a single axis while keeping all other degrees of freedom fixed. The axis is subject to a spring-like restoring torque so that the robot remains upright at equilibrium. In our device, there are two such axes—pitch and roll—so that both can be trimmed simultaneously. When the wings are flapped, they in general, produce both a thrust and a torque. Our device is designed so that applied torque, such as an undesirable bias torque $\tau_b$, results in rotation in proportion to its magnitude. Whereas its design insures that thrust has no effect on rotation, regardless of magnitude. Trimming the robot then consists of determining the direction and magnitude of compensating trim torque $\tau_t$ that reduces rotation approximately to zero.

For our system to operate in this way, we must make the following assumptions about the thrust vector:

1) Its direction is nearly coincident with the body Z-axis
2) It is nearly collinear with the axis of rotation of the flexure joint (that is, the lateral offset $O_R$ shown in Fig. 2 is small).

We will later show, in Section IIIC, how our device design includes a calibration process in which the robot is precisely positioned to insure assumption (2) above holds.

In our device, we use an integrating feedback control loop to find the compensatory trim torque $\tau_t$. The dynamical equation for how the system's rotation angle evolves with time is:

$$J\ddot{\theta} = \tau_b - k_s\theta - c\dot{\theta} + \tau_t \tag{1}$$

Here $J$ is the moment of inertia of the combined robot-trimming device system, $\theta$ is the rotation angle, $\tau_b$ and $\tau_t$ are the bias torque and trim torque respectively, $k_s$ is a spring-like stiffness constant (derived below), and $c$ is a rotational damping coefficient due to aerodynamic drag forces on the flapping wings and damping in the flexure joints. We can solve for the angle at steady-state, giving

$$\theta = \frac{1}{k_s}\left(\tau_b + \tau_t\right). \tag{2}$$

This shows that the only way to make the angle zero is to make $\tau_b = \tau_t$. This provides a means to determine that the robot is trimmed, without the need to know the exact value of $k_s$. Practical design considerations limit the range of $k_s$, which we address below. If we can measure the angle $\theta$ of the robot in the trimming device, for example by using a motion capture camera or an on-board accelerometer, then we can use an integral controller to integrate this error in time to drive it to zero:

$$\tau_t = k_i \int_0^t (\theta_d - \theta)\, dt, \tag{3}$$

where $k_i$ is the integral controller constant and $\theta_d$ is the desired angle, which is zero in our case. This concept can be used for finding both roll and pitch trim torques.

### B. Mechanisms of Torque Actuation

For torque trimming, we are not concerned with the exact mechanism by which a bias torque $\tau_b$ arises, but we must have the means to compensate for it using a trim torque $\tau_t$. In both quad-rotor and flapping-wing platforms, pitch and roll torques can be actuated approximately independently. In a quad-rotor, if rotor speeds are changed, the resulting differential force between propellers causes a torque (Fig. 3). Roll torques in the FIRs are produced through a similar means, by increasing the thrust magnitude of one wing ($T_1$) relative to the other wing ($T_2$),

$$\tau_{roll} = (T_1 - T_2)b.$$

A pitch torque is produced by altering the position of the stroke-averaged center of aerodynamic thrust (Fig. 3),

$$\tau_{pitch} = (T_1 + T_2)d.$$

For a vehicle actuated by other means, such as four electro-hydrodynamic thrusters [9] [8], actuation is very similar to quad-rotor devices.

### C. Restoring Torque and Flexures

A flexure joint is a form of hinge that allows a rotation over a limited range [22]. Pin joints, bearings, and bushings are not suitable for small scale applications, due to friction scaling [23]. Accordingly, rotation in our trimming device is through flexure joints. A simplified, two-dimensional free-body diagram of the device is shown in Fig. 4. The resulting torque on the system, neglecting bias and trim torques, can be calculated using a moment balance and is equal to $k_f\theta - m_R g l_R \sin\theta + m_b g l_b \sin\theta$, where $l_R$ and $l_b$ are the moment arm of the robot and balancing weight from the pivot point respectively, $k_f$ is the stiffness of the flexure joint, and $m_R$ and $m_b$ are the mass of the robot and counter-balance weight respectively. If we linearize the system using

2377-3766 (c) 2019 IEEE. Personal use is permitted, but republication/redistribution requires IEEE permission. See http://www.ieee.org/publications_standards/publications/rights/index.html for more information.

This article has been accepted for publication in a future issue of this journal, but has not been fully edited. Content may change prior to final publication. Citation information: DOI 10.1109/LRA.2020.2967318, IEEE Robotics and Automation Letters



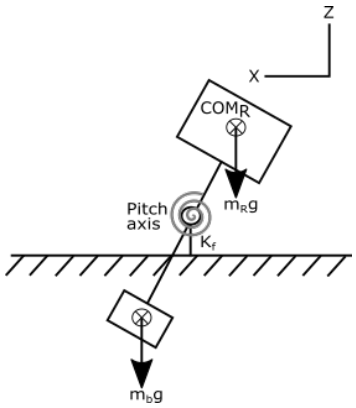


Fig. 4: Free-body diagram of a robot allowed to rotate around a single axis. A counterbalance $m_b$ and torsional spring $k_f$ due to flexure stiffness cause a restoring moment to keep the robot's mass $m_R$ to rest at a near-vertical inclination at equilibrium.

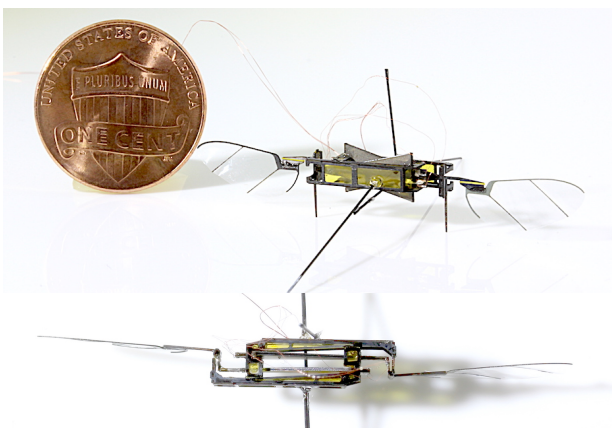

Fig. 5: (top) We have redesigned the Robofly to simplify fabrication by further reducing the number of parts relative to [6] (U.S. penny coin shown for scale).

small-angle approximations around $\theta = 0$, we can write the equivalent stiffness as

$$k_s = k_f - m_R g l_R + m_b g l_b. \tag{4}$$

The restoring torque approaches zero as $\theta$ approaches zero. Therefore, for a properly-trimmed system ($\tau_b = \tau_t$), $k_s$ does not play a role in trim torque calculations. For practical purposes, however, to ensure that the deflections due to typical bias torques can be measured from our motion capture cameras, $k_s$ must not be too large. This is done by choosing the appropriate value of $k_f$.

In early exploratory investigations, we constructed a trimming device with a negative $k_s$, that is, without a counterbalance mass $m_b$. Under these conditions, the system did not have an equilibrium at $\theta$ but instead, the robot rested at the limit of rotation, tilted. Under these conditions, the integral controller performed a "wind-up" until the integrated commanded torque exceeded what was necessary to drive the robot away from its tilted configuration. But with a negative spring constant, the required torque is maximum at that point, and the robot immediately flipped to the other tilted extreme. This repeated

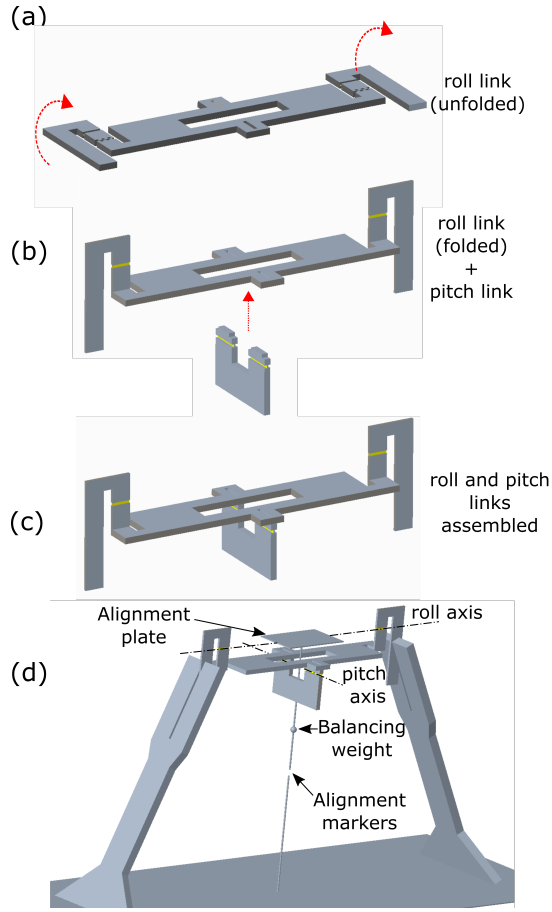


Fig. 6: (a) The roll link of the trimming device. The link is folded around the castellated joint so the fly can be held perpendicular to the roll flexure and parallel to the ground. (b) The pitch link of the device. Its attached to the roll link via protrusions on top. (c) The whole assembly of trimming device, the fly is attached to the pitch link on the bottom. (d) Trimming device attached with the support columns, alignment fixtures and balancing weight.

indefinitely back and forth as the integrator repeatedly wound up. This could be eliminated by adding a proportional component with the requisite spring-like restoring moment, but we chose the more expedient and practical solution of adding the balancing mass $m_b$. This had the additional advantage of allowing for the calibration step to eliminate $O_R$ described in Section IIIC below.

## III. Experimental Apparatus

### A. New Robot Design: Robofly-Expanded

As one of our contributions here, we introduce a new iteration of the Robofly design [6], called Robofly Expanded, that further simplifies fabrication. The new design integrates the wing hinge and legs directly into the main layup, reducing the part count for a complete Robofly, when legs are counted, from 12 in [6], to only 8, and far below the 18 of [1]. Additionally, the actuators are re-oriented so that their long axis is horizontal. This has two desirable results. First, by moving the wings farther apart from each other, torque around

2377-3766 (c) 2019 IEEE. Personal use is permitted, but republication/redistribution requires IEEE permission. See http://www.ieee.org/publications_standards/publications/rights/index.html for more information.

This article has been accepted for publication in a future issue of this journal, but has not been fully edited. Content may change prior to final publication. Citation information: DOI 10.1109/LRA.2020.2967318, IEEE Robotics and Automation Letters



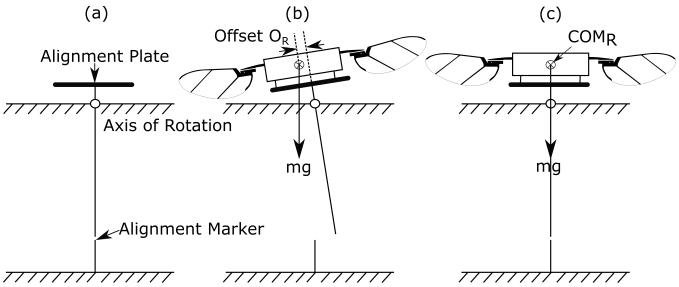


Fig. 7: (a) To align the center of mass of the robot with the axis of rotation of the device, we positioned an "alignment marker" just below a long rod. (b) The robot was then manually placed on a small "alignment plate" made of FR4 at the top of the connecting rod. Any lateral offset $O_R$ causes rotation; the robot is carefully moved laterally in small increments with tweezers until the marks line up again for both pitch and roll axes, as shown in (c), greatly reducing the lateral offset $O_R$.

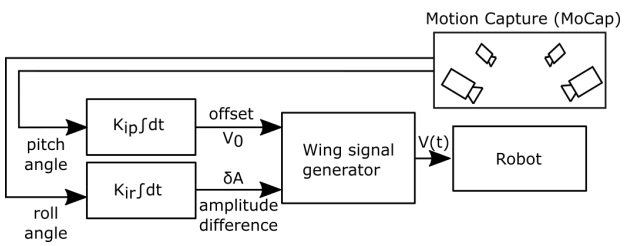


Fig. 8: The control loop used in the trimming device generates the trim voltages by numerically integrating the error in roll and pitch angles estimated by motion capture cameras. The error signals are fed through a signal generator (Simulink real-time), converted to analog, amplified by piezo amplifiers, and fed to the piezo actuators driving the wings.

a vertical, or yaw axis is increased. This is necessary because the only known yaw actuation mode for this basic design consists of actuating the wing faster in one direction than the other to achieve a drag differential. However, this is known to produce a weak force [24]. Increasing the moment arm increases the net yaw force. In [4], this was shown to be sufficient to achieve consistent yaw actuation in either direction, something that was not possible in the design of [1]. Secondly, it allows for increased maneuverability in other directions, by orienting the long axis along the direction of greatest torque, the roll axis [21], and having a very little moment of inertia around its pitch axis. Measurements of pitch torque showed that they were substantially lower than roll torque, by a factor of approximately two [21]. A completed device is shown in Fig. 5.

### B. Trimming Device Design

We chose as our performance specification a maximum bias torque error of 0.3 $\mu$Nm. This is motivated by the estimated torque uncertainty induced by the thin wire tether that provides power and control signals to the robot. While it is hard to provide a simple model of its effect due to its widely variable conformation, one reasonable model for the tether is a torsional spring. Experiments performed in [13] indicated that a 45° rotation causes a torque of approximately 0.3 $\mu$Nm, which we set as our maximum error.

We then used our performance target to design the size of the flexure joints. Flexures were made of 12 $\mu$m polyimide film ("kapton"). The bending stiffness of the flexure joint, is calculated by using $k_f = \frac{Et^3w}{12L}$ [22]. Here, $t$ is the thickness of the flexure material, $L$ is the length of the flexure joint (500 $\mu$m), $w$ is the width of the joint (3 mm) and $E$ is Young's modulus of 2.5 Gpa. At these values, the resulting flexure stiffness is 2.16 $\mu$Nm/rad. The same value of flexure stiffness is used for both roll and pitch joints. With this stiffness, a bias torque of 0.3 $\mu$Nm produces a rotation of approximately 8°. This is easily measured by the motion capture arena, which can measure angles to within approximately 1°, indicating that our device can provide the necessary accuracy. Note that we chose the counter-balance mass and position (Fig. 4) so that $m_b l_b \approx m_R l_R$ so that their equivalent stiffness counteracted the "negative stiffness" caused by the robot's COM being above the flexure rotation axis.

To mitigate buckling, all flexures were loaded in tension rather than compression. The remaining rigid structure was machined from inexpensive, rigid 254 $\mu$m fiberglass (FR4), which sandwiched the polyimide flexure material on both sides, following "smart composite microstructure" fabrication methods first introduced in [25]. A rigid part connects the two perpendicular pitch and roll flexures, which are designed so that their rotation axes are as close as possible to the robot's COM (Fig. 6 (b)), up to 10 mm for the pitch axis. This can cause an error torque if the true thrust vector direction deviates from vertical, violating assumption 1. Adaptive controllers, e.g. in [1], [4], typically estimate this to be about 2°. This results in an error of approximately 0.3$\mu$Nm, within the specification. This could be eliminated in a future revision that brings these flexures nearly perfectly coincident with the COM, but would require parts to physically surround the Robofly's wings, which extend farther than the $\approx$ 50 mm cutting range of the galvanometer of our laser machining system. The robot is mounted on the moving part of the pitch link through a connecting rod. The width of the roll link is minimized, at just 15 mm, so that it does not affect airflow from the wings.

### C. Calibration/Positioning the Robot

Here we describe features of our trimming device that allow us to minimize $O_R$, the lateral displacement between the thrust vector and the trimming device's flexure-based rotation axis (Fig. 2(a)). Without this step, we found that trim estimates exhibited large errors, manifested in free-flight as large undesirable rotational accelerations at takeoff. To understand how a non-zero offset $O_R$ could introduce error in our measurement, consider the case of robot displaced laterally by a small amount, such as $O_R$=1 mm, on the trimming device. If thrust $T$ is equal to the mass of the vehicle, $T = mg$ = 1.2 mN, then the error in torque measurement $T \times O_R$ is 1.2 $\mu$Nm. This is large compared to our 0.3 $\mu$Nm accuracy target, and therefore represents a source of error that must be eliminated.

Our solution is to use the mass of the robot itself as the source of information about its positioning. If the wings are

2377-3766 (c) 2019 IEEE. Personal use is permitted, but republication/redistribution requires IEEE permission. See http://www.ieee.org/publications_standards/publications/rights/index.html for more information.

This article has been accepted for publication in a future issue of this journal, but has not been fully edited. Content may change prior to final publication. Citation information: DOI 10.1109/LRA.2020.2967318, IEEE Robotics and Automation Letters



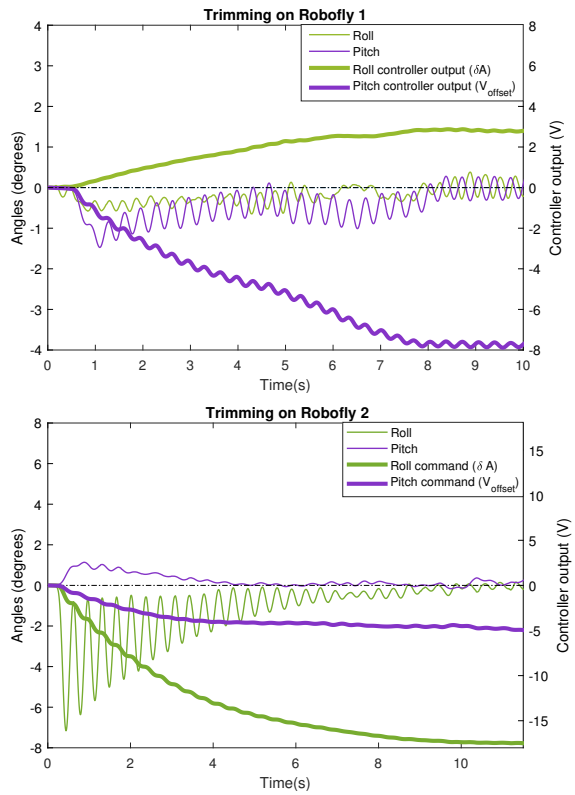


Fig. 9: Results from trials on two different Robofly devices in the trimming device. Left axes show the angles of the two rotation axes as measured by motion capture, which are driven to zero by the integrating action of the feedback controller. Right axes show how the compensating bias voltages evolve in time as the trimming device settles on the correct trim values.

not flapping, then a lateral displacement of its COM ($O_R$ in Fig. 2(a)) induces a torque about the flexure due to gravity acting on the robot's body. Hence, the calibration procedure consists of moving the robot laterally on the trimming device until its pitch and roll angles are equal to what they were before the robot was added as shown in (Fig. 7). After the robot is in its calibrated position, its feet are carefully glued to the surface with cyanoacrylate glue on a temporary basis. A soldering iron is used to carefully melt the glue and remove the robot when it is ready to fly.

### D. Fabrication

Parts were machined using a diode-pumped solid state (DPSS) laser with a wavelength of 355 nM (Photomachining, Inc., Massachusetts). The roll link includes "castellated" cuts, which permit precise specification of the rotation axis, which are glued to a fixed angle as part of the assembly process (Fig. 6 (a)). Layers were pin-aligned and bonded together using a thermal sheet adhesive (18 $\mu$m Pyralux FR-1500) using a heat press at 200 C under a force of 50 kg. A subsequent release cut separated the required links from scaffolding. The assembly process is shown in Fig. 6 (b) in which the two links are glued together. These are bonded to a stable base that holds

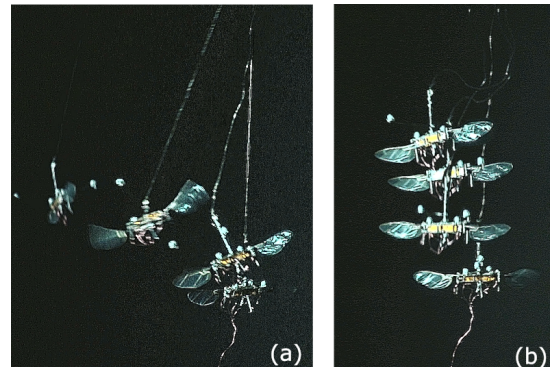


Fig. 10: (a) Video-composite images taken from an untrimmed open-loop takeoff of Robofly (offset voltage $V_o$ and voltage differential $\delta A$ at 0 V). (b) Open-loop of the same robot using trim values derived from the trimming device from the trimming procedure in Fig. 9(top). The robot lifts off nearly vertically, producing clearly-discernible slack in the kevlar restraining filament at the top. The vertical flight indicates that the vehicle has been properly trimmed.

the assembly away from the surface of the table at about 15 cm to minimize the ground effect due to the table surface below. A lightweight scaffold is then added to hold the retroreflective motion capture markers. The complete device with a Robofly is shown in Fig. 1.

### E. Trimming Controller

A diagram showing the essential components of the closed-loop trimming system is shown in Fig. 8. The motion capture system (four Prime13 cameras, OptiTrack, Inc., Salem, OR) sends the orientation of the trimming device in quaternion form over Ethernet at 240 Hz. A computer running Simulink Real-Time (Mathworks, Natick, MA) performs control computations and produces an analog voltage waveform that is amplified using piezo amplifiers (Trek model 2205). The control computer calculates Euler angles roll $\theta_x$ and pitch $\theta_y$ from the quaternion, with a convention matching those of the flexures in the trimming device. The displacement of the wings varies linearly with the voltage applied to the piezo actuators, with the voltage signal to the left and right wings being

$$\begin{aligned} V_l(t) &= (A+\delta A)\sin(\omega t)+V_o+V_b/2 \\ V_r(t) &= (A-\delta A)\sin(\omega t)+V_o+V_b/2, \end{aligned}$$

respectively. Thrust varies approximately linearly with flapping amplitude [26]. Here, $A$ is the baseline voltage amplitude, $\omega$ is the flapping frequency, and $V_b$ is the piezo bias voltage. Roll torque is varied by varying $\delta A$, the amplitude difference between left and right wings. Pitch torque is varied by varying $V_o$, the mean voltage of the sinusoid. To avoid actuator breakage due to cracks, the controller includes saturation blocks to limit the range of these inputs [27].

## IV. Results

### A. Trimming Results

Voltage commands from the integral controller and output angles measured by motion capture for two different Robofly

2377-3766 (c) 2019 IEEE. Personal use is permitted, but republication/redistribution requires IEEE permission. See http://www.ieee.org/publications_standards/publications/rights/index.html for more information.

This article has been accepted for publication in a future issue of this journal, but has not been fully edited. Content may change prior to final publication. Citation information: DOI 10.1109/LRA.2020.2967318, IEEE Robotics and Automation Letters



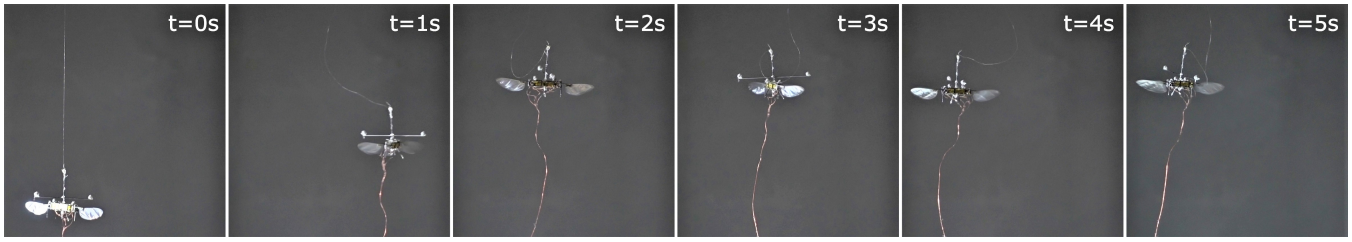


Fig. 11: Snapshots of hovering Robofly. The fly is controlled by an altitude and a lateral controller running in parallel. The trimming values used in the controller were obtained from the trimming device in the trimming procedure shown shown in Fig.9 (top).

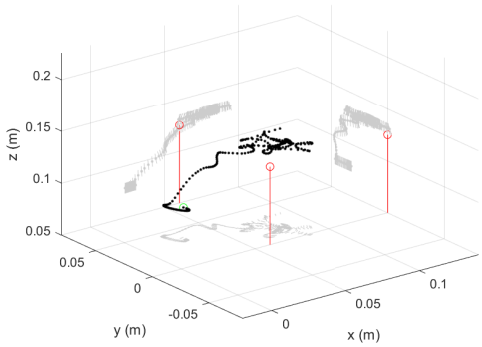


Fig. 12: 3D trajectory of Robofly while hovering. The red circle shows the desired position in space. Black markers indicate the position of the robot spaced at intervals of 0.05 s. Projections of the trajectory, including its attitude, are shown in grey at the sides of the figure.

devices are shown in Fig. 9. In both cases, trim voltages appear to asymptotically reach steady-state values within approximately 10 s. Resulting trim values are a pitch offset voltage $V_o$=-8 V and amplitude differential $\delta A$=3 V for the first and $V_o$=-5 V, $\delta A$=-17 V for the second. These results show that the system can arrive at a calibration regardless of the polarity of the bias torque.

To establish whether trimming was successful, we compared open-loop flights before and after trimming. In both cases, the wings were driven with a flapping frequency of 150 Hz and amplitude of 180 V. The device was constrained by a thin Kevlar thread to minimize crashes. For un-trimmed flights, $V_o = V_d = 0$. A video-composite of frames from an untrimmed flight shows that the robot exhibits large attitude deviation and soon flies out of the frame (Fig. 10 (a)). Using the trim voltages obtained from the trimming device, the robot can be observed to take off nearly vertically, indicating a properly-trimmed device (Fig. 10 (b)). Similarly, the second Robofly exhibited an equivalent transition from tumbling to vertical flight after trimming.

### B. Hovering

We confirmed that the trimming values from our trimming device could be used for hovering flight as well. We used the controller derived from [4] and [7], which is an evolution of the one used in [1]. As in many controllers for underactuated systems, the controller operates by tilting the thrust vector in the desired direction to perform lateral motions [4], [28]. The first Robofly was commanded to hover at a height of 12 cm for 5 seconds. It was able to hover successfully using trim values from the trimming device with position RMS error of 21, 18 and 6 mm in x, y and z directions, respectively. The resulting 3D trajectory can be seen in Fig. 12. The second Robofly also successfully hovered using its trim values from the trimming device at the height of 21 cm for 5 seconds with position RMS errors of 17, 49 and 7 mm in x, y and z directions respectively. Frames from the video of first Robofly are shown in Fig. 11. Videos of the trimming process on the device and open and closed-loop flights are provided in the supplementary video, as well as hovering results for both Roboflies tested.

## V. Conclusion and Future Work

In this letter, we present a device for correcting the bias torques that are almost always present in small-sized airborne robots due to manufacturing irregularity in their complex flapping mechanics. Calibration is usually not required for rotorcraft like quad-rotor helicopters because their bias torques are typically much smaller. Our device operates in a feedback control loop using motion capture feedback. We performed validation experiments on two different Robofly devices, successfully trimming them. In both cases, before the devices were trimmed, they exhibited strong pitch and roll torque in free flight, tumbling almost immediately after take-off. The entire trimming process took less than 25 minutes including calibration, and less than fifteen seconds of wing flapping time. Compared to manual trimming, where the trimming time and number of airborne flights depends on the operator skill, our process is automatic, more predictable and causes less wear. After trimming, both devices were observed to lift off nearly vertically and did not tumble. Trim values consisted of commanded voltage offsets to the drive waveform of the piezo actuators. Subsequently, we showed that our estimated trim values could be used by our controller to perform stable hovering flight. By greatly speeding and automating an essential yet time consuming step in robot fly fabrication, our device will facilitate high volume manufacturing of FIRs.

Our device is also able to trim robots with a payload such as a battery or sensor package not perfectly centered relative to the COM. Misalignment is equivalent to a nonzero $O_R$ that is corrected for using the calibration procedure in Fig. 7. An alternative way to build the trimming device is by tethering the robot to a thin metal rod. Although simple, this method

2377-3766 (c) 2019 IEEE. Personal use is permitted, but republication/redistribution requires IEEE permission. See http://www.ieee.org/publications_standards/publications/rights/index.html for more information.

This article has been accepted for publication in a future issue of this journal, but has not been fully edited. Content may change prior to final publication. Citation information: DOI 10.1109/LRA.2020.2967318, IEEE Robotics and Automation Letters



would result in large estimation errors in the event that the thrust vector was not perfectly aligned with the body z-axis, because of the large moment arm.

Yaw trimming could be added by incorporating a vertical-axis flexure between the alignment plate and connecting rod. This addition would not be subject to the potential for the confounding thrust-induced torque that required calibration for the pitch and roll axes, making it a simple addition. Thrust force trimming could also be added by placing the entire device on a sensitive balance scale, positioning the lightweight robot and trimming device off of the side of the scale to minimize the aerodynamic ground effect. Furthermore, it is possible to measure the spring constants of the trimming device's flexures by adding small known weights and measuring deflection. Knowing these, aerodynamic torques can be measured directly. This could be used to perform comprehensive characterization of aerodynamic characteristics, such as how torques vary with flapping frequency or amplitude, to improve control performance.

While our system was shown in operation on two-winged devices, its design accommodates other designs, such as 4-winged robots [4], or micro-robots actuated by other thruster types such as electrohydrodynamic thrusters [9].

The trimming device presented in this letter uses a camera-based motion capture system to measure orientation on the trimming device, but this is not a requirement. It is expected that most fully-autonomous robots will incorporate an inertial measurement unit (IMU) onboard [29]. The accelerometer in the IMU can serve as an inclinometer on the trimming device, precisely measuring the rotation angle for both pitch and roll axes in place of the motion capture system.

## Acknowledgment

This work is partially supported by the Air Force Office of Scientific Research under grant no. FA9550-14-1-0398.

## References

[1] K. Y. Ma, P. Chirarattananon, S. B. Fuller, and R. J. Wood, "Controlled flight of a biologically inspired, insect-scale robot," *Science*, vol. 340, no. 6132, pp. 603–607, 2013.

[2] H. V. Phan, Q. V. Nguyen, Q. T. Truong, T. Van Truong, H. C. Park, N. S. Goo, D. Byun, and M. J. Kim, "Stable vertical takeoff of an insect-mimicking flapping-wing system without guide implementing inherent pitching stability," *Journal of Bionic Engineering*, vol. 9, no. 4, pp. 391–401, 2012.

[3] C. T. Orlowski and A. R. Girard, "Dynamics, stability, and control analyses of flapping wing micro-air vehicles," *Progress in Aerospace Sciences*, vol. 51, pp. 18–30, 2012.

[4] S. B. Fuller, "Four wings: An insect-sized aerial robot with steering ability and payload capacity for autonomy," *IEEE Robotics and Automation Letters*, vol. 4, no. 2, pp. 570–577, 2019.

[5] X. Yang, Y. Chen, L. Chang, A. A. Calderón, and N. O. Pérez-Arancibia, "Bee$^+$: A 95-mg four-winged insect-scale flying robot driven by twinned unimorph actuators," *CoRR*, vol. abs/1905.02253, 2019. [Online]. Available: http://arxiv.org/abs/1905.02253

[6] Y. M. Chukewad, A. T. Singh, J. M. James, and S. B. Fuller, "A new robot fly design that is easier to fabricate and capable of flight and ground locomotion," in *2018 IEEE/RSJ International Conference on Intelligent Robots and Systems (IROS)*. IEEE, 2018, pp. 4875–4882.

[7] Y. M. Chukewad, J. James, A. Singh, and S. Fuller, "Robofly: An insect-sized robot with simplified fabrication that is capable of flight, ground, and water surface locomotion," 2020.

[8] D. S. Drew, N. O. Lambert, C. B. Schindler, and K. S. Pister, "Toward controlled flight of the ionocraft: a flying microrobot using electrohydrodynamic thrust with onboard sensing and no moving parts," *IEEE Robotics and Automation Letters*, vol. 3, no. 4, pp. 2807–2813, 2018.

[9] E. Dedic, Y. M. Chukewad, R. S. Vaddi, I. Novosselov, and S. B. Fuller, "A laser-microfabricated electrohydrodynamic thruster for centimeter-scale aerial robots," 2019.

[10] P. Chirarattananon, K. Y. Ma, and R. J. Wood, "Adaptive control of a millimeter-scale flapping-wing robot," *Bioinspiration & biomimetics*, vol. 9, no. 2, p. 025004, 2014.

[11] V. Kumar and N. Michael, "Opportunities and challenges with autonomous micro aerial vehicles," *The International Journal of Robotics Research*, vol. 31, no. 11, pp. 1279–1291, 2012.

[12] B. Cheng, X. Deng, and T. L. Hedrick, "The mechanics and control of pitching manoeuvres in a freely flying hawkmoth (manduca sexta)," *Journal of Experimental Biology*, vol. 214, no. 24, pp. 4092–4106, 2011.

[13] S. B. Fuller, M. Karpelson, A. Censi, K. Y. Ma, and R. J. Wood, "Controlling free flight of a robotic fly using an onboard vision sensor inspired by insect ocelli," *Journal of The Royal Society Interface*, vol. 11, no. 97, p. 20140281, 2014.

[14] S. Balasubramanian, Y. M. Chukewad, J. M. James, G. L. Barrows, and S. B. Fuller, "An insect-sized robot that uses a custom-built onboard camera and a neural network to classify and respond to visual input," in *2018 7th IEEE International Conference on Biomedical Robotics and Biomechatronics (Biorob)*. IEEE, 2018, pp. 1297–1302.

[15] J. James, V. Iyer, Y. Chukewad, S. Gollakota, and S. B. Fuller, "Liftoff of a 190 mg laser-powered aerial vehicle: The lightest wireless robot to fly," in *2018 IEEE International Conference on Robotics and Automation (ICRA)*. IEEE, 2018, pp. 1–8.

[16] N. Jafferis, E. Helbling, M. Karpelson, and R. Wood, "Untethered flight of an insect-sized flapping-wing microscale aerial vehicle," *Nature*, vol. 570, pp. 491–495, 06 2019.

[17] P. Chirarattananon, K. Y. Ma, and R. J. Wood, "Adaptive control for takeoff, hovering, and landing of a robotic fly," in *2013 IEEE/RSJ International Conference on Intelligent Robots and Systems*. IEEE, 2013, pp. 3808–3815.

[18] R. W. Yeung, "On the interactions of slender ships in shallow water," *Journal of Fluid Mechanics*, vol. 85, no. 1, pp. 143–159, 1978.

[19] R. C. Nelson *et al.*, *Flight stability and automatic control*. WCB/McGraw Hill New York, 1998, vol. 2.

[20] G. D. Padfield, *Helicopter flight dynamics*. Wiley Online Library, 2008.

[21] K. Y. Ma, S. M. Felton, and R. J. Wood, "Design, fabrication, and modeling of the split actuator microrobotic bee," in *2012 IEEE/RSJ International Conference on Intelligent Robots and Systems*. IEEE, 2012, pp. 1133–1140.

[22] R. Malka, A. L. Desbiens, Y. Chen, and R. J. Wood, "Principles of microscale flexure hinge design for enhanced endurance," in *2014 IEEE/RSJ International Conference on Intelligent Robots and Systems*. IEEE, 2014, pp. 2879–2885.

[23] R. J. Wood, B. M. Finio, M. Karpelson, K. Y. Ma, N. O. Pérez-Arancibia, P. S. Sreetharan, H. Tanaka, and J. P. Whitney, "Progress on "pico" air vehicles," in *ISRR*, 2011.

[24] N. Gravish and R. J. Wood, "Anomalous yaw torque generation from passively pitching wings," in *2016 IEEE International Conference on Robotics and Automation (ICRA)*. IEEE, 2016, pp. 3282–3287.

[25] A. M. Hoover, E. Steltz, and R. S. Fearing, "Roach: An autonomous 2.4 g crawling hexapod robot," in *2008 IEEE/RSJ International Conference on Intelligent Robots and Systems*. IEEE, 2008, pp. 26–33.

[26] N. O. Pérez-Arancibia, K. Y. Ma, K. C. Galloway, J. D. Greenberg, and R. J. Wood, "First controlled vertical flight of a biologically inspired microrobot," *Bioinspiration & Biomimetics*, vol. 6, no. 3, p. 036009, 2011.

[27] R. Wood, E. Steltz, and R. Fearing, "Optimal energy density piezoelectric bending actuators," *Sensors and Actuators A: Physical*, vol. 119, no. 2, pp. 476–488, 2005.

[28] A. Roberts and A. Tayebi, "Adaptive position tracking of vtol uavs," *IEEE Transactions on Robotics*, vol. 27, no. 1, pp. 129–142, 2010.

[29] S. B. Fuller, E. F. Helbling, P. Chirarattananon, and R. J. Wood, "Using a mems gyroscope to stabilize the attitude of a fly-sized hovering robot," in *MAV 2014: Int. Micro Air Vehicle Conf.and Competition 2014, Delft, The Netherlands*. Citeseer, 2014.

2377-3766 (c) 2019 IEEE. Personal use is permitted, but republication/redistribution requires IEEE permission. See http://www.ieee.org/publications_standards/publications/rights/index.html for more information.